Fast, Fine-grained, and Robust Grouping of RFIDs

Meng Jin*†
Shanghai Jiao Tong University
jinm@sjtu.edu.cn

Kexin Li*
Shanghai Jiao Tong University
likexin0103@sjtu.edu.cn

Xiaohua Tian
Shanghai Jiao Tong University
xtian@sjtu.edu.cn

Xinbing Wang
Shanghai Jiao Tong University
xwang8@sjtu.edu.cn

Chenghu Zhou
Chinese Academy of Sciences
zhouch@lreis.ac.cn

ABSTRACT

This paper presents the design, implementation, and evaluation of TaGroup, a fast, fine-grained, and robust grouping technique for RFIDs. It can achieve a nearly 100% accuracy in distinguishing multiple groups of closely located RFIDs, within only a few seconds. It would benefit many inventory tracking applications, such as self-checkout in retails and packaging quality control in logistics.

We make two technical innovations. First, we propose a novel method which can measure the channels between multiple pairs of commercial RFID tags simultaneously, and then estimate the proximity relations between them based on the channel information. Second, we introduce a spatio-temporal graph model which captures a full picture of proximity relations among all the tags, based on which TaGroup can perform a robust grouping of the tags. These two designs together boost the grouping speed and accuracy of TaGroup. Our experiments show that in grouping 120 tags into 4 closely located groups, TaGroup can achieve a nearly 100% accuracy, at the cost of only 3 seconds.

CCS CONCEPTS

• **Computer systems organization → Sensor networks**.

KEYWORDS

RFID, Wireless Sensing, Inventory Tracking

*Co-primary authors
†Corresponding author

ACM MobiCom '23, October 2–6, 2023, Madrid, Spain

ACM ISBN 978-1-4503-9990-6/23/10…$15.00
https://doi.org/10.1145/3570361.3592510

1 INTRODUCTION

Radio-frequency identification (RFID), as one of the top 10 influential technologies in the 21st century [5], is widely used in various fields, such as logistics, supply chains, retails, and so on. In all those fields, inventory tracking is a core operation, where fast and accurate identification of proximity RFID groups (e.g., listing the items in each sealed box) could be a game-changer. For example, today's packaging quality control ends once the boxes are sealed. While, since many of today's products are already tagged with RFIDs, an accurate grouping of the RFIDs would enable the system to further check whether the right item is in the right box. Another example is self-checkout in retail stores. Today's system requires the customer to pass through the CA one at a time. If accurate RFID grouping is achieved, we can allow multiple consumers pass through the CA simultaneously, and the system can distinguish the items in different shopping bags.

A potential enabler for the above applications is RFID localization[14, 16, 17, 20, 21, 25, 27, 28, 33]. By attaching the container (e.g., the box) with a reference tag and localize both the reference tag and the tagged items, we can distinguish the RFIDs in different containers. Unfortunately however, today's RFID localization is fragile to many practical factors such as multipath reflection, NLoS signal propagation, and coupling between nearby tags [24], which are inevitable in inventory scenarios where numbers of RFID-tagged items are shoved into boxes or shopping bags. So, although the recent localization techniques have reported centimeter-level accuracy, such an accuracy is hard to achieve in our scenarios. Besides, some high-accuracy RFID localization methods [16, 21] will cost seconds to localize one tag, which is clearly unacceptable in inventory applications where tens or hundreds of tags need to be grouped within seconds.

We in this paper solve the above problem with TaGroup, a system which performs fast, accurate, and robust RFID grouping by directly detecting the physical proximity among tags, bypassing the intractable localization problem. The design of TaGroup is based on a technique which can build a "channel" between two commercial RFID tags. Specifically, some recent works [12] reveal that when two tags transmit

simultaneously, one tag reflects not only the signal from the reader, but also that from the other tag, resulting in inter-tag backscattering. So, by simultaneously querying two tags, we can build a channel between them. The inter-tag channel is highly sensitive to the inter-tag spacing, and thus can be used as a sensitive indicator to capture the physical proximity among tags. During the inventory process, we can accumulate plenty of such inter-tag channels and construct a full picture of the proximity relation among all the tags. Based on such a picture, we can perform a robust RFID grouping.

TaGroup introduces three innovations that together allow it to achieve accurate, robust, and fast RFID grouping:

(a) Accurate proximity detection: TaGroup's first technique innovation allows it to accurately estimate the proximity between tags based on their superposed signal. Specifically, we first provide a technique to isolate the inter-tag reflection from the superposed signals and cancel out other interferences therein (i.e., the reflections from individual tags, the ambient reflections, and the coupling effect between tags). Then, based on the extract inter-tag reflection, we propose a metric, named *RF-bond*, to reliably capture the proximity between tags. We prove through theoretical analysis and empirical studies that RF-bond is highly sensitive to the inter-tag distance and is immune to coupling effect and multipath.

(b) Robust RFID grouping with a proximity relation graph: RFID localization methods locates a tag based only on the tag-reader channel, which makes them brittle to errors in channel measurement. TaGroup's advantage is that it can leverage many more channels. Specifically, by combining the RF-bond obtained over space (between different pairs of tags) and time (across different reading rounds), TaGroup can build a spatio-temporal graph, named *PRG* (proximity relation graph), which captures the proximity relation among all the tags. Then the RFID grouping problem can be formulated as a graph based clustering problem, where the clustering result is obtained based on a joint consideration of the RF-bonds among all the tags, and can be refined through the evolution of the graph during inventory process.

(c) Parallel proximity relation measuring. To achieve a highly efficient RFID grouping, a fast measurement of the proximity relations among tags is important. TaGroup boosts this process with its third innovation – a technique that can measure the RF-bond among multiple pairs of tags in parallel. Specifically, we first design a series of protocol-compatible reader commands which can query multiple tags in parallel. Then we design a signal resolving method, which can extract the inter-tag channel between each two tags simultaneously. Our experimental results show that we can support as high as four simultaneously transmitting tags, which means that we can obtain $\binom{4}{2} = 6$ proximity relations in parallel. This increases the RFID grouping speed by multiple times.

Contributions. TaGroup makes three contributions:

- Leveraging the inter-tag channel, we propose a new form of RFID localization where the localization problem is transformed to a graph-based grouping problem.
- We propose a robust and fast RFID grouping system TaGroup, which involves: i) a method to accurately extract the inter-tag channels among multiple pairs of tags in parallel; ii) a metric (*RF-bond*) that accurately reflects the proximity relation between tags; iii) a graph model (PRG) that captures the proximity relations among tags over time and space; and iv) an graph-based grouping algorithm that fuses the information contained in PRG for robust RFID grouping.
- We build a prototype of TaGroup and extensively evaluate its performance under a full range of configurations. Experiment results show that in grouping 120 tags into 4 closely located groups, TaGroup can achieve a nearly 100% accuracy, at the cost of only 3 seconds.

2 RELATED WORK

2.1 RFID Localization

Recent advances in RFID localization have achieved cm-level accuracy [3, 12, 14, 16, 21, 25, 27], which makes them a potential solution for accurate RFID grouping. Unfortunately, none of them can deliver on the accuracy or efficiency requirements for inventory tasks. Specifically, most of them achieve such a high localization accuracy by combining the signal collected from different spatial locations [3, 12, 21, 25, 27] or frequencies [16, 20]. To localize a tag, they need to either move their antenna over multiple meters or perform frequency hopping over a large bandwidth, both of which cost several seconds. Consider that an inventory tracking systems usually need to track tens or hundreds of tags concurrently, these localization method will incur prohibitively-high (can be as high as several minutes) tracking delay.

Besides localization delay, another problem is that they cannot provide the required accuracy in practical retail and logistic environments. Specifically, most of them do not explicitly tackle the inter-tag coupling effect caused by dense deployment, which could undermine the localization metrics (e.g., RSSI and phase) and thus impact the reported localization accuracy. The experimental results in [24] tells that even a fairly low level of phase or RSSI measurement error can result in a meter-level range localization error, which can easily lead to an incorrect grouping result.

2.2 RFID-based Inventory Tracking

There are some existing works focus on a similar scenario (i.e., inventory tracking) with TaGroup. For example, RFGo [2] proposes a RFID based self-checkout system. However, different from TaGroup, RFGo can only determine whether a tag is inside the checkout area, so it requires the consumers

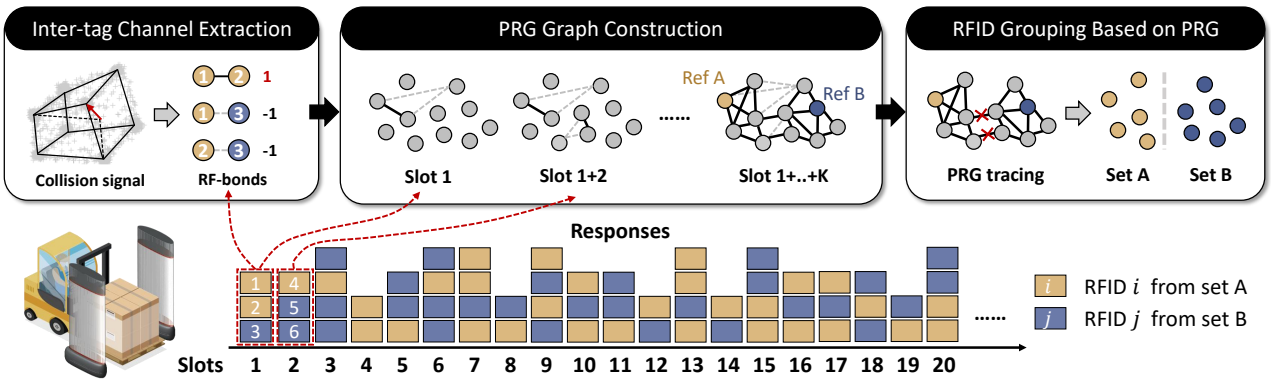

Figure 1: Overview.

to pass through the checkout area one by one, while TaGroup allows them to pass through simultaneously.

In comparison, Taggo [4] and STPP [21] can distinguish items in different shopping baskets and thus allow multiple baskets to pass through the checkout area simultaneously. However, besides the problem of coupling effect mentioned in Sec. 2.1, another key problem underlying both of them is that they require the tags to move along a straight line with a stable speed, and then sort the tags based on the order they passing through the reading antenna. This is clearly not the case in inventory scenarios where the mobility of the customers or the forklifts can be highly random.

3 OVERVIEW

TaGroup is an accurate and fast RFID grouping system which achieves a nearly 100% accuracy in grouping hundreds of tags within 3s. It works even when the tags suffer serious multipath and coupling effect during the inventory process.

Following a common practice in RFID based inventory, TaGroup assumes that the items are tagged with RFIDs. Further, TaGroup also need to attach one (or multiple if required) reference RFIDs on the containers of the items (e.g., on the shopping bags).

Fig. 1 shows the architecture of TaGroup. At a high level, it performs RFID grouping through the following three steps:

- TaGroup continuously query both the on-item tags and the references. The tags response randomly following the Slotted Aloha protocol as shown in Fig. 1. At each query slot TaGroup could receive simultaneous responses from a random subset of those tags (say M tags), and extracts the $\binom{M}{2}$ inter-tag channels from the superposed signal.
- TaGroup builds RF-bonds among tags based on the extracted inter-tag channels, and generates the PRG graph by accumulating the RF-bonds obtained across spatial (different pairs of tags) and time (different query slots).
- TaGroup models RFID grouping as a graph-based clustering problem and assign each RFID to the correct set by tracing the RF-bonds on the PRG graph.

The next few sections elaborate on the above steps, providing the technical details.

4 INTER-TAG CHANNEL EXTRACTION

4.1 Understanding the PHY-layer of RFID

In an RFID system, the reader antenna A sends a carrier wave S_0, and the tag T responds its data $x(t)$ by reflecting or absorbing the carrier wave using OOK modulation (see Fig. 2). The signal received at the reader is represented as:

$$S(t) = h_T \cdot x(t) \cdot S_0,$$

where $x(t) = 0$ or 1 represents the encoded bits. $h_T = h_{A \leftarrow T} h_{T \leftarrow A} = \alpha e^{\mathrm{j}\delta}$ denotes the signal's *channel distortion* along the round-trip propagation path, where α and δ denote the *amplitude attenuation* and *phase rotation* during the propagation, respectively.

Observed on the IQ domain, the signal forms two points (as shown in Fig. 3(a)), corresponding to the silence (L) and the reflecting (H) states of the tag. The *length* and *direction* of the vector $\vec{S_T}$ connecting these two points represents the amplitude α and phase δ of the tag's signal, respectively. Many existing backscatter-based sensing techniques use those two metrics to estimate a target's location [33], orientation [1], mobility [7, 9, 19, 35], material [30], etc.

In practice, however, besides the tag's reflection, the reader also receives two sources of additional interference signals:

- **Ambient reflection.** Ambient reflection refers to the signal reflected from the objects in the environments, which can be categorized into two types: i) the *background reflection*, which refers to the signal that is directly reflected by the environmental objects; and ii) *multipath reflection*, which refers to the signal reflected from the tag, bouncing off of different objects in the environment, then arriving

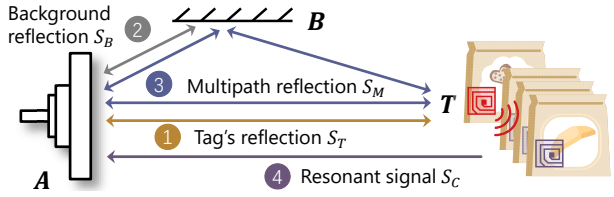

Figure 2: Signal propagation of one tag.

at the receiver. We denote background reflection and multipath reflection as S_B and S_M, respectively.

- **Coupling effect.** Coupling effect occurs between two close-by tags, where signals reflected from a responding tag generate resonant voltage in the other silent tags [29, 31] (as shown in Fig. 3). So, besides the responding tag, the silent tags also emit resonant signals. We treat the resonant signals from all the nearby tags as if they were from one virtual tag. Then, the reader will further receive an additional source of signal, denoted as S_C.

The final signal received by the reader is a superposition of three sources of signals: the LoS reflection from the tag, the ambient reflection, and the resonant signal. We have:

$$S(t) = (h_M + h_T + h_C) \cdot x(t) \cdot S_0 + h_B \cdot S_0 \tag{1}$$

where $h_M = h_{A\leftarrow B} h_{B\leftarrow T} h_{T\leftarrow A}$, $h_B = h_{A\leftarrow B} h_{B\leftarrow A}$, and h_C denote the channel of the multipath reflection, background reflection, and the superposed resonant signals.

The above discussion tells that due to the impact from multipath and coupling effect, the extracted channel parameters (i.e., phase and amplitude) of the signal are typically distorted from the real value. This is why some existing localization methods suffer poor accuracy in practical scenarios.

4.2 Extracting the inter-tag channel

Now we consider our scenario where we simultaneously query multiple tags and extract the inter-tag channel between each two of them. Ideally, when M tags transmit simultaneously, the received signal S is a superposition of all the M tags' signals S_{T_i} ($1 \le i \le M$), along with their multipath reflections S_{M_i} and resonant signals S_{M_i}. We have:

$$S(t) = \sum_{i=1}^{M} (h_{M_i} + h_{T_i} + h_{C_i}) \cdot x_i(t) \cdot S_0 + h_B \cdot S_0 \tag{2}$$

This superposed signal will form 2^M signal vectors on IQ domain, representing the signals obtained on 2^M different combined states of the tags. Figs. 5(a) and 5(b) show the examples with two and three tags. In Fig. 5(a), the $2^2 = 4$ points represent the four combined states of the tags, namely L_1L_2, H_1L_2, L_1H_2 and H_1H_2.

Actually, when multiple tags transmit simultaneously, a tag reflects not only the reader's signal, but also the signal from other nearby tags, incurring the so called inter-tag

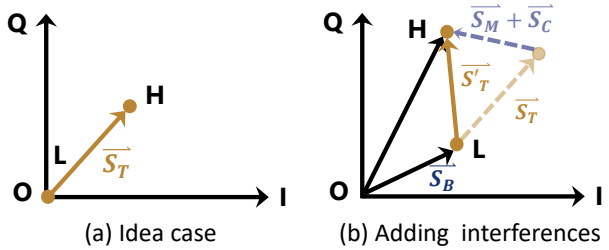

Figure 3: Signal propagation of one tag.

reflection. So, besides the signals considered in Eq. (2), the reader will further receive $\binom{M}{2}$ additional signals, which are the inter-tag reflection between each two tags (as shown in Fig. 4). Due to the inter-tag reflection, the received signal is further expressed as:

$$S(t) = h_B \cdot S_0 + \sum_{i=1}^{M} (h_{M_i} + h_{T_i} + h_{C_i}) \cdot x_i(t) \cdot S_0 + \underbrace{\sum_{i=1}^{M} \sum_{j=1}^{M} h_{INT}^{(i,j)} \cdot x_i(t) x_j(t) \cdot S_0}_{\text{Inter-tag reflection } S_{INT}^{(i,j)}} \tag{3}$$

where the third term is the inter-tag reflection between each two tags T_i and T_j, denoted as $S_{INT}^{(i,j)}$ ($i \neq j$). We denote the inter-tag channel as $h_{INT}^{(i,j)} = 2h_{A\to T_i} h_{T_i\to T_j} h_{T_j\to A}$.

Now, a natural problem is: how can we extract the inter-tag reflection $S_{INT}^{(i,j)}$ between each two tags from the superposed signal? We achieve this based on the observation in [12] that for each two tags T_i and T_j, the inter-tag reflection occurs only when both of them are in the reflecting state (i.e., when $x_i(t)x_j(t) = 1$). So, in the IQ domain, vector $\vec{S}_{INT}^{(i,j)}$ is contained only in the signal vector where both T_i and T_j are on H state. For example, in the case with two tags, $\vec{S}_{INT}$ is contained only in $\vec{S}_{H_1H_2}$ (see Fig. 5 (c)); in the case with three tags, $\vec{S}_{INT}^{(1,2)}$ is contained only in $\vec{S}_{H_1H_2H_3}$ and $\vec{S}_{H_1H_2L_3}$ (see Fig. 5 (d)). Then by observing the differential of signals on different states, the receiver can isolate the inter-tag reflection.

Equations (4) and (5) give an example of how we can extract S_{INT} from the collided signal of two tags. Specifically, when there are two tags transmit in parallel, the signal on each combined state can be represented as:

$$\begin{aligned}
\vec{S}_{H_1H_2} &= (\vec{S}_{T_1} + \vec{S}_{M_1} + \vec{S}_{C_1}) + (\vec{S}_{T_2} + \vec{S}_{M_2} + \vec{S}_{C_2}) + \vec{S}_{INT} + \vec{S}_B \\
\vec{S}_{H_1L_2} &= \vec{S}_{T_1} + \vec{S}_{M_1} + \vec{S}_{C_1} + \vec{S}_B \\
\vec{S}_{L_1H_2} &= \vec{S}_{T_2} + \vec{S}_{M_2} + \vec{S}_{C_2} + \vec{S}_B \\
\vec{S}_{L_1L_2} &= \vec{S}_B
\end{aligned} \tag{4}$$

Based on the above equation, we can obtain $\vec{S}_{INT}$ as:

$$\vec{S}_{INT} = \vec{S}_{H_1H_2} - \vec{S}_{H_1L_2} - \vec{S}_{L_1H_2} + \vec{S}_{L_1L_2} \tag{5}$$

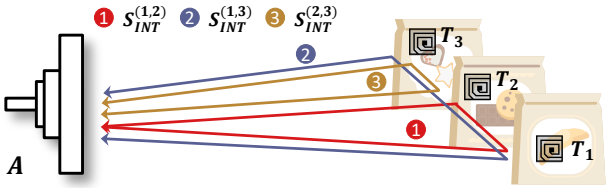

Figure 4: Inter-tag reflection.

Then we consider the case with M tags. To isolate the inter-tag reflection between each two tags $S_{INT}^{(i,j)}$, we need to find the state where both T_i and T_j are on the H state while other tags are on L state. We denote the corresponding signal vector as $\vec{S}_{T_iT_j}$. We also need to find the two states where only one of the two tags (i.e., T_i or T_j) is on the H state (which are denoted as $\vec{S}_{T_i}$ and $\vec{S}_{T_j}$). Then the inter-tag reflection $S_{INT}^{(i,j)}$ can be obtained as:

$$\vec{S}_{INT} = \vec{S}_{T_iT_j} - (\vec{S}_{T_i} + \vec{S}_{T_j}) + S_B \tag{6}$$

Fig. 5 (c) shows the superposed signal of three tags, where, for example, the inter-tag reflection between T_1 and T_2 can be extracted as $S_{HHL} - (S_{LHL} + S_{HLL}) + S_{LLL}$.

The above discussions reveal an important property of inter-tag reflection:

Property 1. *The inter-tag reflection is naturally resilient to interferences such as multipath reflection and coupling effect, which makes it a reliable metric for fine-grained localization.*

4.3 State Identification

Sec. 4.2 tells that, to obtain the inter-tag reflection, we need to first identify the combined state of each signal vector (e.g., to identify which signal vector in Fig. 5 (c) represents signal $\vec{S}_{HH}$). This can be achieved leveraging the existing parallel decoding [8, 11, 18, 26] and channel extraction methods [10, 22, 32]. In our design, we use FlipTracer [11] to identify the 2^M combined states and then use Eq. (6) to extract the inter-tag reflection S_{INT} between each two tags.

5 RFID GROUPING

TaGroup performs RFID grouping based on the proximity relation among tags, which is captured by a graph model named PRG (Proximity-Relation-Graph). We denote PRG as $\mathbf{PRG} = (\mathbf{T}, \mathbf{B})$, where $\mathbf{T} = \{T_i | 1 \le i \le N\}$ denotes the tags to be inventoried. $\mathbf{B} = \{B_{i,j} | 1 \le i \le j \le N\}$ denotes the RF-bond between each two tags T_i and T_j, which reflects the proximity between them.

In this section, we first introduce how we build a RF-bond between two tag based on the inter-tag channel. Then, we introduce how we can generate the PRG by cumulating the RF-bonds obtained across spatial and time. Finally, we perform RFID grouping based on the constructed PRG.

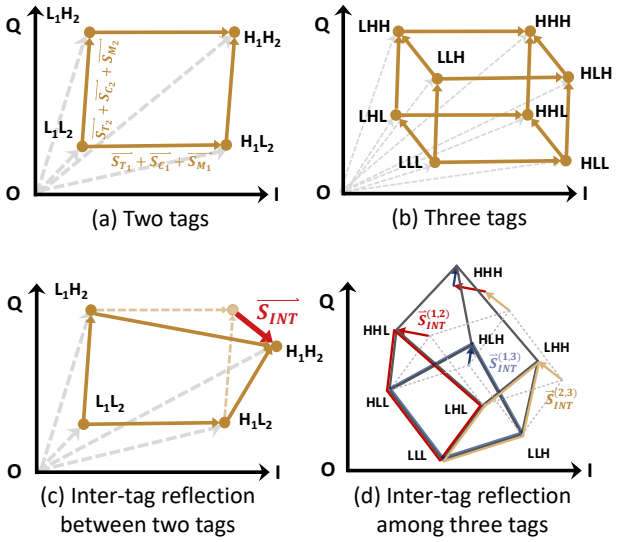

Figure 5: Superposed signal on IQ domain.

5.1 Building the RF-bond among tags

To transform the inter-tag channel to a metric which captures the proximity relation between tags, we first perform an experiment to observe how the inter-tag distance affects the inter-tag channel. Fig. 6 (a) shows the deployment detail of the experiment. We change the distance between two tags from 5cm to 80cm, during which we fix the reader-tag distance at 1.5m. Fig. 6 (b) shows the amplitudes of the inter-tag reflections (i.e., α_{INT}) measured under different inter-tag distances. As can be seen, α_{INT} increases monotonously with a decreased distance. This implies that α_{INT} can effectively reflect the distance between the two tags. However, we cannot directly use α_{INT} to quantify the inter-tag distance since α_{INT} is indeed determined by the signal's attenuation on three channels as

$$\alpha_{INT} = 2 \cdot \alpha_{A \to T_1} \alpha_{T_1 \to T_2} \alpha_{T_2 \to A}.$$

Besides the inter-tag distance $d_{T_1 \to T_2}$, α_{INT} is also affected by the antenna-tag distances, i.e., $\alpha_{A \to T_1}$ and $\alpha_{A \to T_2}$.

To observe the impact of antenna-tag distance, we repeat the above experiment by fixing the reader-tag distance at 2m. The results is shown in Fig. 6 (b). By comparing the results obtained at 1.5m and 2m, respectively, we find that α_{INT} is indeed dominated by the inter-tag distance. This is because that the inter-tag distance is much smaller than the antenna-tag distance. Consider that signal's amplitude decays with the square of the propagation distance, signal amplitude is more sensitive to the change in distance when the distance itself is smaller (as shown in Fig. 7). In other words, with a same change in $d_{A \to T_1}$ (or $d_{A \to T_2}$) and $d_{T_1 \to T_2}$, the change in $\alpha_{T_1 \to T_2}$ is more obvious than that in $\alpha_{A \to T_1}$ (or $\alpha_{A \to T_2}$).

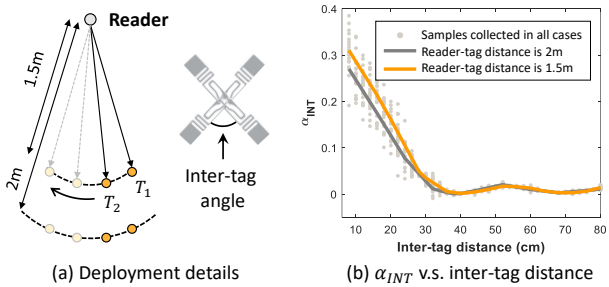

(a) Deployment details (b) α_{INT} v.s. inter-tag distance

Figure 6: Inter-tag channel v.s. inter-tag distance

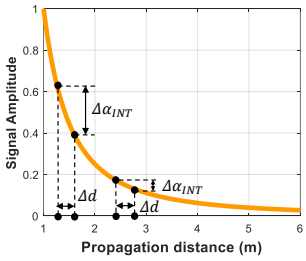

Figure 7: α v.s. d.

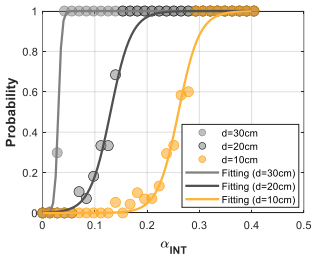

Figure 8: P_ϵ v.s. α_{INT}.

We further repeat the above experiments under different inter-tag angles (from 0° to 180°, with a step of 30°), as shown in Fig. 6 (a). The gray dots in Fig. 6 (b) show the α_{INT} v.s. $d_{T_1 \to T_2}$ measured under different angles. As can be seen, although α_{INT} measured under the same inter-tag distance varies across tag orientations and antenna-tag distances, it can still reflect the distance between the two tags. So, although we cannot use α_{INT} to quantitatively measure the inter-tag distance, we can still use it to *qualitatively* capture the proximity relation between tags.

Specifically, we capture the proximity relation between two tags with a probabilistic function $P_\epsilon(\alpha_{INT})$, which means *the probability that the inter-tag distance is lower than a given value ϵ when the measured amplitude of the inter-tag reflection is α_{INT}*. For example, $P_{10}(0.15) = 70\%$ means that when $\alpha_{INT} = 0.15$, there is a 70% probability that the inter-tag distance is smaller than 10cm. Here, ϵ is an application-related parameter, which is configured by the application layer.

To determine the probabilistic function $P_\epsilon(\alpha_{INT})$, we perform extensive experiments to observe the amplitude of inter-tag channel α_{INT} under different inter-tag distances (from 5cm to 80cm), tag-antenna distances (from 120cm to 250cm), and inter-tag angles (from 0° to 180°). Based on the experimental results, Fig. 8 statistically shows how $P_\epsilon(\alpha_{INT})$ changes with α_{INT} when ϵ is set at $10cm$, $15cm$, and $20cm$. The characteristic "S" shape of the curves indicates that $P_\epsilon(\alpha_{INT})$ is an effective and sensitive metric in detecting the proximity between two tags. We fit $P_\epsilon(\alpha_{INT})$ with a logistic function as:

$$P_\epsilon(\alpha_{INT}) = \frac{1}{1 + e^{-k(\alpha_{INT} - \alpha_0)}}$$

where k and α_0 are the two parameters which capture the steepness and midpoint of the curve, respectively. The fitting results shown in Fig. 8 tell that the logistic function well approximates this relationship.

Based on P_ϵ, we propose the RF-bond metric which captures the proximity relation between two tags i and j. Specifically, RF-bond is calculated by normalizing P_ϵ to the range of $[-1, 1]$ as:

$$Bond_\epsilon(T_i, T_j) = 2 \cdot P_\epsilon(\alpha_{INT}^{i,j}) - 1 \tag{7}$$

Here, a positive RF-bond indicates a close proximity between the two tags, vice versa.

5.2 PRG Construction

PRG graph is constructed based on the RF-bonds among tags obtained during the inventory process. In an inventory process, the reader divides a time frame into $K = 2^Q$ slots (Q is a system parameter) and each tag randomly picks a slot to reply its ID, as shown in Fig. 9. At a slot where multiple, say M, tags respond simultaneously, the reader extracts the $\binom{M}{2}$ inter-tag channel from the superposed signal, using the technique in Sec. 4, and then builds the RF-bond between each two tags, using the technique in Sec. 5.1. The tags that are not successfully queried in the current frame will be left to the next frame. Each query round ends when all the tags are queried. TaGroup repeats the query process for several rounds to collect sufficient proximity relation information in the PRG graph.

The PRG construction process is divided into two phases: the *initialization phase* and the *update phase*. The target of the initialization phase is to generate a connected PRG. Specifically, TaGroup check the connectivity of the constructed PRG at the end of each query round. Once a connected PRG is constructed, TaGroup ends the initialization phase and forward the constructed PRG to the following grouping module. If the grouping module find that the information contained in the PRG is insufficient to support confidential grouping, it will trigger the update phase, where a new round of query is issued to collect more information. The mechanism to trigger the update phase is introduced in Sec. 5.3.

Speed up the PRG construction. We further propose a method to speed up the PRG construction process. Specifically, consider that TaGroup can process at most four tags in parallel, the PRG construction speed can be maximized if all the slots are filled with exactly four tags. However, since each tag selects the time slot randomly, we cannot control the number of tags in each slot. So, to maximize the efficiency,

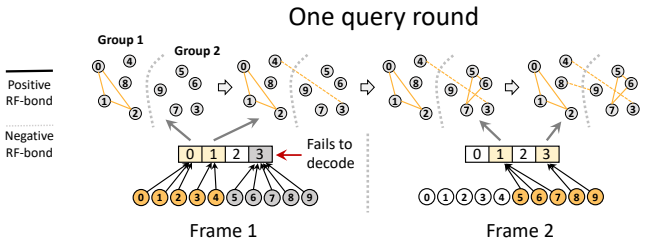

Figure 9: The process in generating the PRG graph.

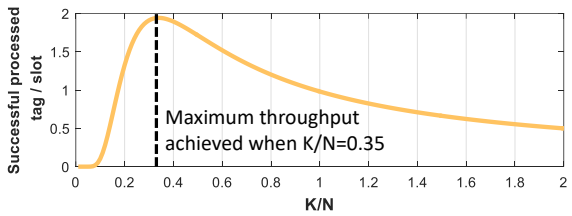

Figure 10: Expected throughput under different K/N.

we should find a optimal frame size K, so that the average number of tags in each slot is optimized.

Specifically, given the frame size K and the tag number N, the expected number of slots with M tags can be expected as

$$E_M = K\binom{N}{M}(\frac{1}{K})^M(1-\frac{1}{K})^{N-M} \tag{8}$$

Given that TaGroup can process at most four tags in parallel, the average throughput (successfully processed tags per slot) can be estimated as:

$$Th = \sum_{M=1}^{4} M \cdot K\binom{N}{M}(\frac{1}{K})^M(1-\frac{1}{K})^{N-M} \tag{9}$$

Fig. 10 shows the averaged throughput depending on frame size to tag ratio K/N. As can be seen, the maximum throughput is achieved if we set $K = 0.35 \cdot N$.

One problem is that the tag number N is not known initially. To solve this problem, we initialize N as the average of the history value in pervious inventory tasks. At the end of the first query round, the reader can make an estimation of the tag number, based on which, it can select a optimal frame size K for the following query rounds.

Two points are worth noting here:

- We cannot guarantee that every pair of tags can be ever queried simultaneously during the inventory process. For two tags i and j which have never been queried simultaneously, we cannot obtain their inter-tag channel and thus their proximity relation. In this case, we set the RF-bond between them as $Bond(T_i, T_j) = 0$.
- The reader may also obtain the RF-bond between two tags multiple times on different slots during the inventory process. In this case, we set their RF-bond as the maximum value obtained in the whole process.

5.3 RFID grouping based on PRG

Now we have the PRG graph, which describes the proximity relation among tags. The next target is to group the N tags into N_S different sets based on the PRG graph. We denote the reference tags as $\{R_1, ..., R_{N_S}\}$. Then, a naive solution here is to group each tag based on its proximity relations (i.e., RF-bonds) to the reference tags. However, a problem is that, in most cases, we cannot obtain a complete graph that captures the proximity relation between each two tags. Besides, although we can obtain a complete proximity relation between a tag and all the references, grouping the tags solely based on the references is not robust enough.

To solve the above problem, we propose to group the tags in an incremental fashion. Specifically, we for each tag propose a metric to quantify how *confident* the algorithm can group it to a correct set. Then we group the tags in order of their confidence levels. Tags with higher confidence level will be grouped earlier, and then be used as new references to group the tags with lower confidence level. In this way, those low-confidence tags can be grouped based on a joint consideration of more references, which helps to produce a more reliable and credible grouping result. An toy example of this method is shown in Fig. 11, where we group 9 tags to three sets in a incremental fashion.

One problem here is how to evaluate the confidence level of a tag. We propose to quantify it based on the distribution of the tag's proximity relations to all the sets. Our insight is: the more significant that a tag is proximate to a certain set with respect to others, it is more confident in grouping the tag to that set. Otherwise, if a tag shows similar proximity level to multiple sets or does not provide sufficient proximity relation information for decision making, the grouping algorithm will identify it as a low-confidence tag.

Based on the above consideration, we define the confidence in grouping a tag T_i to a set S_s as:

$$C(T_i, S_s) = PX_s(T_i) - \sum_{j \neq s} PX_j(T_i) \tag{10}$$

where $PX_j(T_i)$ denotes a tag T_i's proximity relation to a set S_j, which is initialized as its RF-bond with the corresponding reference R_j (i.e., $PX_j(i) = Bond(T_i, R_j)$). Eq. (10) tells that a tag T_i shows a high confidence to a set S_s only when: i) it shows a high proximity level to Reference R_s while a low proximity level to all the other references; and ii) we can obtain a relative complete information on its proximity relation to different sets (with more non-zero PX in Eq. (10)).

Then, Tag T_i's confidence level is estimated as:

$$Conf(T_i) = max(C(T_i, \mathbf{S})) - second\_max(C(T_i, \mathbf{S})) \tag{11}$$

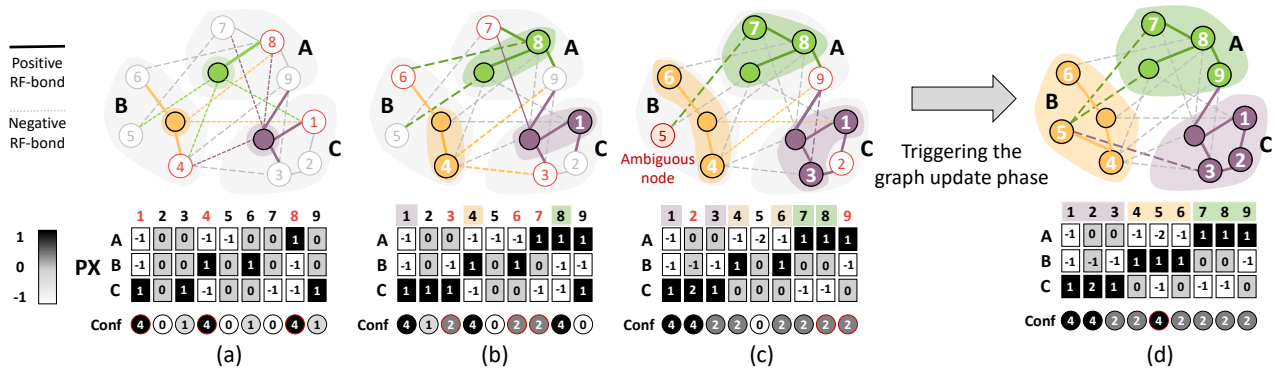

Figure 11: The process in grouping 9 tags to three different sets. Figs (a)-(d) shows the assignment on each iteration and the updated proximity relation between the 9 tags and three sets after each iteration.

where $second\_max(C(T_i, S_j))$ denotes the second maximum value in $C(T_i, S_j)$. Eq. (11) tells that a tag T_i shows a high confidence level only when it shows a skewed proximity level to a certain set.

In each iteration of the grouping process, we select the top-t confident tags and group them to the corresponding sets. In the example shown in Fig. 11, we have $t = 3$, and the top-3 high-confidence tags in the first iteration are T_1, T_4, and T_8, which show high confidence to sets S_C, S_B, and S_A, respectively. After grouping the top-t tags, we can treat them as new references. Then we will have multiple references in each set. Now for a tag T_i, its proximity relation to a set S_j can be estimated based on a joint consideration of its proximity relation with all the references in that set. Specifically, for a set S_j which have Re references, denoted as $\{R_j^1, ..., R_j^{Re}\}$, we can calculate a tag T_i's proximity relation to set S_j as:

$$PX_j(T_i) = \frac{\sum Bond(T_i, R_j^{re})}{Re}$$

Based on this updated proximity relation, we can further update the confidence metric of each tag, then find out new high-confidence tags, and group them to different sets. We repeat this process until all the tags have been grouped.

The bottom figures in Fig 11 show the proximity relations between the 9 tags and the three sets on each iteration. As can be seen, with more tags are added as reference tags, the tags' proximity level PX is more skewed to a certain set, and then the grouping algorithm can make a more credible decision on which set a tag belongs to.

Triggering the PRG update phase. Note that TaGroup cannot determine the assignment of a tag if its confidence level keeps at 0. This means that the tag always shows equal confidence levels to multiple sets. We term such tag as an *ambiguous tag*. For example, in Fig. 11, we have never obtained Tag 5's proximity relation to Sets B and C. Thus its PX value to these two sets keeps at 0, and also its confidence level. So, in a grouping process, if an ambiguous tag is detected, TaGroup will trigger the PRG update phase to obtain more proximity relations for more confident decision making.

6 MAC LAYER PROTOCOL

We meet a problem in integrating TaGroup into the standard EPC-Gen2 protocol for RFIDs. In the standard protocol, the reader initiates a session by sending a Query command to the tags. After successfully decode the Query, the tags contend for the channel by first sending a 16-bit random signal (i.e., RN16) at a randomly selected time slot. If the RN16 is successfully decoded by the reader, the reader ACKs the tag by responding it with the same RN16 signal and then the tag responds its EPC ID to the reader. In the case where M tags transmit simultaneously, however, although TaGroup can successfully decode the RN16 of all the M tags and get the $\binom{M}{2}$ RF-bonds among the tags based on the collided RN16 signals, it can only response to one of the M tags and gets its EPC, as shown in Fig. 12. That is to say, the reader cannot identify the other $M - 1$ tags.

To solve this problem, we leverage the fact that a tag's PHY-layer features can also be used as an identity [15, 23, 34]. Specifically, due to manufacturing and tag location diversities, signal emitted by different tags show different PHY-layer features. We propose to use tags' *frequency errors* and *channel parameters*, two features that can be extracted from the collided RN16 signal, as a fingerprint to distinguish different tags in one query round. With such a PHY-layer identity, we can distinguish different tags without their EPC ID.

In the following of this section, we first introduce the workflow of TaGroup's communication protocol, which is designed on top of the standard EPC-Gen2 Protocol. Then we introduce the signal features which we used for tag identification in the protocol.

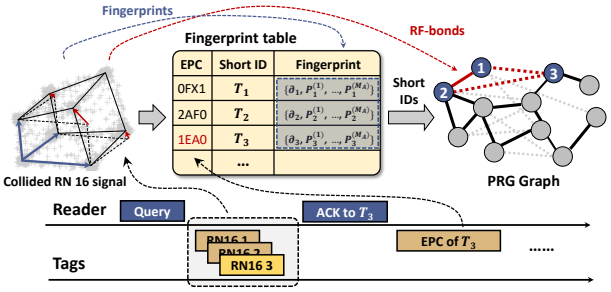

Figure 12: TaGroup's tag identification process.

6.1 Protocol workflow

Fig. 12 illustrates the detailed workflow of TaGroup's tag identification process. In our design, each tag has one fingerprint and two IDs (a EPC ID and a short ID), all of which are stored in a fingerprint table, as shown in Fig. 12. Here, the EPC ID is a tag's universal identifier while the short ID is used to denote a tag in the PRG graph. Upon receiving simultaneous transmission from M tags, the receiver first extracts their fingerprints and maps the fingerprints to the corresponding tags (short ID) based on the fingerprint table. Then, TaGroup obtains the $\binom{M}{2}$ RF-bonds between the tags using the techniques introduced in Secs. 4 and 5.1 and updates the PRG graph with the newly obtained RF-bonds. After this, TaGroup randomly selects one in the tags whose EPC ID is not recorded yet (e.g., Tag T_3 in Fig. 12) and ACKs the tag. The tag will response its EPC after receiving the ACK and then the receiver records its EPC in the table. TaGroup repeatedly query the tags multiple rounds, until all the tags' EPCs have been collected.

Note that the fingerprint table is empty initially and is generated and updated during the querying process. Specifically, when the reader obtains a fingerprint that is not contained in the fingerprint table, it considers it as a new tag, adds it to the table, and assigns it with a new short ID.

6.2 Fingerprint extraction

Then we briefly introduce the signal features we used as a fingerprint of a tag and how we can extract the fingerprint of M tags simultaneously from their collided RN16 signal.

Frequency error. A tag's clock exhibits high frequency error (denoted as ∂), resulting differences in tags' clock frequencies [34]. Such a difference further results in the difference in tags' bit durations, i.e., the time between two bit-boundary flips of a tag's signal. TaGroup leverages the method introduced in [18] to extract the flippings of each tag from the collided RN16 signals, and then calculate the bit duration of each tag.

Channel parameters. Due to the difference in tags' locations, orientations, and other physical states, different tags have different channel parameters (i.e., amplitude and phase).

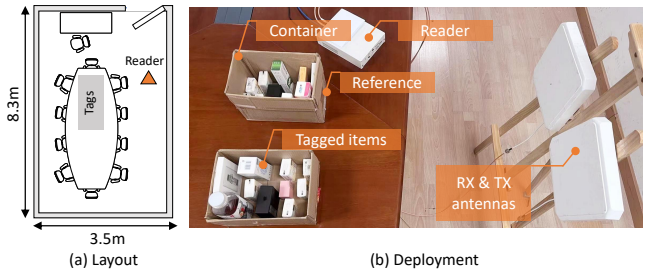

Figure 13: Experiment settings.

So, we can also use channel parameters as a PHY-layer feature to identify the colliding tags. We face two problems here. First, different tags may have similar channel parameters. Second, a tag's channel parameters, which change with the mobility of the tag, cannot serve as a stable tag identity.

We solve the first problem by using multiple antennas. Specifically, for each tag T_i, if we have M_A antennas, we can get M_A channel estimates. It is unlikely that two tags have similar channel estimates on all the M_A antennas.

We solve the second problem leveraging the continuity in tag's channel change. Specifically, based on our observations and the experimental results reported in many existing works [22, 32], the channel of one tag usually changes within some range during the channel coherence time. Even the tag moves in two successive readings, the channel's changes within these period can be still lower than a certain level. So the change in the channel parameters can be still captured if we keep updating the fingerprint table with the newly obtained fingerprints of the tags.

7 EVALUATION

7.1 Experimental Methodology

Reader implementation. We implement TaGroup's reader on USRP N2920 equipped with WBX daughterboards. We adapt a USRP RFID reader developed in [13] and integrate TaGroup's design into the EPC Gen2 protocol as described in Sec. 6. If not mentioned, we deploy only two circularly antennas (Laird S9028PCR ANTENNA, with an 8 dBi gain), one transmitter for sending reader commands and one receiver for capturing tags signal. The reader operates at a carrier frequency of 910 MHz and a ADC sampling rate of 10 MHz.

Commercial RFID tags. Our experiments are performed with the most widely deployed type of RFIDs: the Alien Squiggle RFIDs. Each of these tags costs less than 3 cents.

Environmental setup. We evaluate TaGroup in a fully-furnished indoor environments. Fig. 13 illustrates our experiments' default setup. To simulate the self-checkout and inventory tracking applications, we attach RFID tags to a set of items and put them randomly into different containers. Reference tags are randomly attached on the containers.

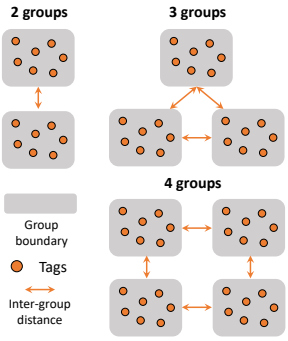

Figure 14: Layout

Figure 15: Three types of containers.

Table 1: Default configurations.

N_S	N_A	N_R	d_{Inner}	d_{Inter}	$d_{A\to T}$[1]
3	1	2	6cm	16cm	1.5m

Note that the locations of the reference tags are not needed to be known in TaGroup. We use three types of containers, i.e., plastic baskets, cloth shopping bags, and cardboard boxes, which are widely used in retails and logistics, as shown in Fig. 15. If not mentioned, we use cardboard box as default. For experiments with different tag scales, we will use boxes with different sizes.

In the experiments, we evaluate the performance of TaGroup under a full range of configurations, including the total number of tags that need to group (N), the number of groups (N_S), the distance between tags in the same group (termed as inner-group distance, d_{Inner}), the distance between two containers (termed as inter-group distance, d_{Inter}), the antenna-to-tag distance $d_{A\to T}$, container's material, and etc. Here, the inner-group distance is roughly calculated as $\frac{\sqrt{A}}{\sqrt{N_S}}$, where A is the area of each group and N_S is the number of tags belong to this group. The define of inter-group distance is illustrated in Fig. 14. We also evaluate how we can improve the grouping accuracy of TaGroup by increasing the number of antennas N_A and the number of reference tags in each group N_R. Table. 1 shows the default configurations and Fig. 14 shows the layout of the tags under different group numbers.

Metric. TaGroup's performance is mainly evaluated by the metric of grouping accuracy, which is defined as the ratio between the number of tags grouped correctly and the tags in total. Besides the grouping accuracy, we also tested TaGroup's grouping latency in Sec. 7.8.

Baseline. We compare TaGroup with two state-of-the-art RFID-based relative positioning methods: STPP [21] and Taggo [4], both of which estimate the relative position of

[1]Here, $d_{A\to T}$ means the distance between the antenna and the nearest tag

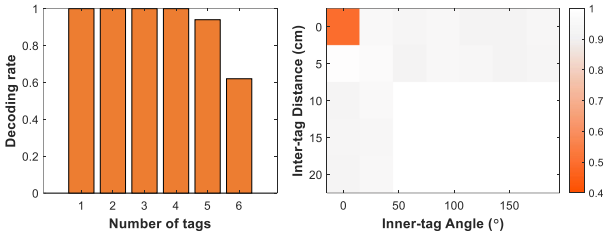

(a) Decoding rate v.s. tag number (b) Impact of inter-tag distance and inter-tag angle

Figure 16: Performance in parallel decoding.

tags based on the tags' phase profiles captured by a moving antenna. To group a tag to a container, both these two methods need to attach at lest four tags on the four upper edges of the container. We implement them a moving antenna which is fixed on a moving robot that moves at 0.3m/s.

7.2 Performance in Parallel Decoding

To build a inter-tag channel, one of the key enabler is TaGroup's ability to decode collided RN16 signals. So we in this section first evaluate TaGroup's performance in parallel decoding.

We first explore the maximum number of tags that TaGroup can support in parallel. Fig. 16(a) shows the decoding rate[2] achieved with different numbers of tags. As can be seen, TaGroup can support at most 5 tags to transmit in parallel.

We further evaluate how the inter-tag distance and inter-tag angle affect the decoding rate. In this experiment, we use two tags. We change the inter-tag distance between them from 0cm to 20cm and the inter-tag angle between them from 0° to 180°. Fig. 16(b) shows the result obtained under different inter-tag distances and inter-tag angles. As can be seen, the decoding rate crashes only when both the inter-tag distance and the inter-tag angle approach 0. This is because that in these cases, at least one of the two tags may become unreadable due to the coupling effect [6]. Note that this a common problem in almost all the RFID systems. Some existing works (e.g., RFGo[2]) have been proposed to solve this problem. TaGroup is compatible with those designs.

7.3 Comparison to State-of-the-Art

Now we compare TaGroup's grouping accuracy to the state-of-the-art techniques described in Sec. 7.1: STPP [21] and Taggo [4]. In this experiment, 60 RFID tags were placed with random orientations in three boxes. We put 20 tags in each box, which is attached with 2 reference tags. The layout of the boxes are shown in Fig. 14. We group the tags using only one antenna. Fig. 17 plots the CDF of the grouping accuracy for TaGroup, STPP, and Taggo.

As can be seen, TaGroup achieves a 100% accuracy (0 error rate) in more than 90% cases, which is highly needed

[2]Number of successfully decoded RN16s in all the transmitted RN16s

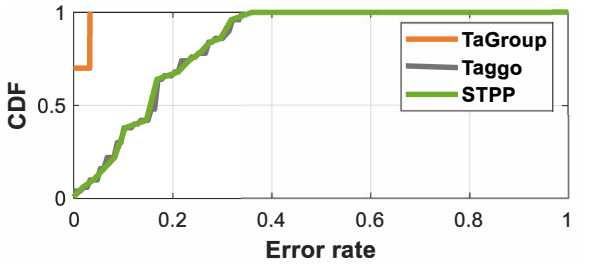

Figure 17: Comparison to State-of-the-Art.

by logistics and retails. In contrast, STTP and Taggo achieves a higher than 90% accuracy (lower than 10% error rate) in only less than 20% cases. Moreover, TaGroup achieves this performance with only one fixed receiving antenna and only two reference tags on each box.

7.4 Performance with more antennas

Now we evaluate the grouping accuracy that TaGroup achieved using more antennas. In this experiment, we put 60 and 120 RFID tags into 2~4 boxes. In each setting of the tag number and group number, we try to group the tags by fusing the PRG obtained by 1~4 antennas. The results in grouping 60 and 120 tags are shown in Figs. 18 (a) and (b), respectively. We observe the following: i) Using two antennas is sufficient to group 60 tags into 4 groups; ii) In the case with 120 tags, the grouping accuracy increases significantly with the number of antennas. This means that TaGroup needs more antennas in grouping more tags. The key reason here is that when the number of tag increases, TaGroup needs more antennas to build more complex fingerprints to distinguish those tags in the tag identification process. This reveals a fact that TaGroup's scalability is limited more by the standard protocol used in RFID systems (which is designed to avoid the collision between tags), but not inherent to our design.

7.5 Performance with more reference tags

We further evaluate how the performance of TaGroup can be improved by adding more reference tags. In the experiment, we tested TaGroup's performance in grouping 60 and 120 tags with 1~3 reference tags in each group. Figs. 19 (a) and (b) show the results. Similar to the case in adding more antennas, adding more references can also increases the grouping accuracy, especially when there are more tags. This is because that adding more reference tags provides TaGroup with more opportunities to get more complete information on tags' proximity relation to the sets. As can be seen, in the case with 60 tags, we can still achieve a 100% accuracy by simply adding more reference tags.

Another important observation is that, in the case with 120 tag, we can hardly get a 100% accuracy even with 3 reference

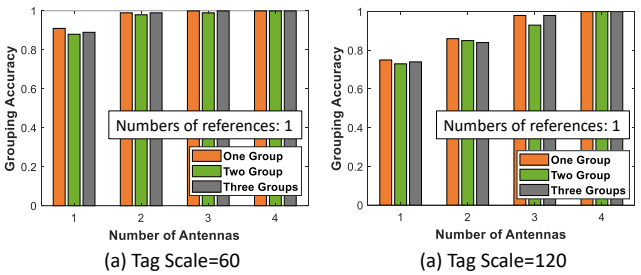

Figure 18: Performance with more antennas.

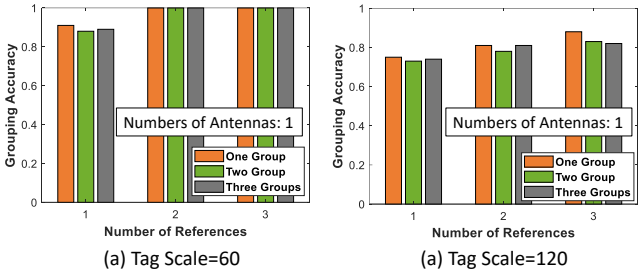

Figure 19: Performance with more references.

tags in each group. The reason is that in the case with 120 tags, we can hardly distinguish the fingerprint of each tag using only one antenna, as we have mentioned in Sec. 6.

7.6 Accuracy v.s. Different Parameters

Next, we would like to evaluate TaGroup's grouping accuracy as a function of different system parameters.

7.6.1 Accuracy v.s. the number of tags. We first evaluate TaGroup's scalability by observing its performance in grouping different number of tags. In this experiment, we use three antennas. The experiment is performed under 5 different tag scales (from 30 to 150, with a step of 30). We put the tags into three containers and each container is attached with two references. The grouping accuracy achieved under different tag scales are shown in Fig. 20.

As can be seen, when using three antennas and two references each group, the maximum tag scale that TaGroup can support is 120. When the tag number reaches 150, the accuracy drops significantly. The reason is explained in Sec. 7.4. It is important to note that, the bottleneck that limits the scalability of TaGroup is the ALOHA-based standard protocol used by RFID systems, but not inherent to our design.

7.6.2 Impact of inter-group distance. Since an important assumption underlying the design of TaGroup is that the inter-group distance is larger than the inner-group distance, we in this experiment evaluate the minimum inter-group distance TaGroup can support. In this experiment, we group 60 tags to 3 groups with 1 antenna. Each group is attached with 2 references. we change the inter-group distance d_{Inter}

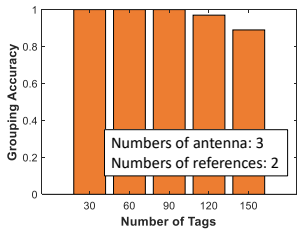

Figure 20: Accuracy v.s. Number of tags.

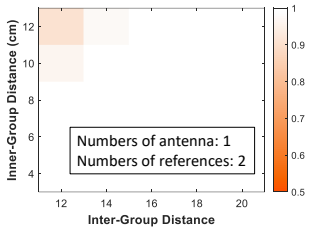

Figure 21: Impact of d_{Inter} and d_{Inner}.

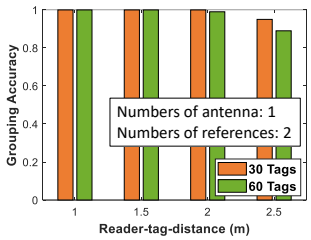

Figure 22: Accuracy v.s. Antenna-to-tag Distance.

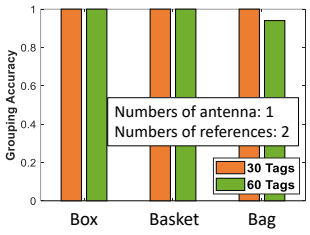

Figure 23: Impact of the container material.

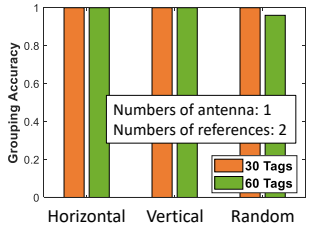

Figure 24: Impact of random tag arrangement.

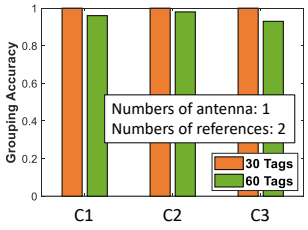

Figure 25: Impact of different obstacles.

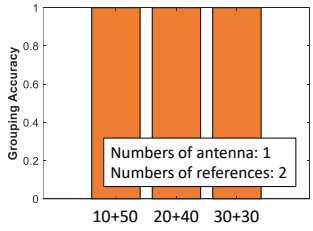

Figure 26: Impact of uneven tag distribution.

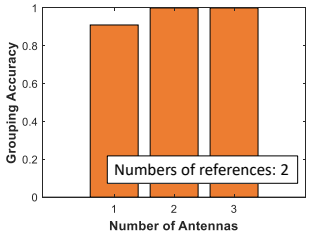

Figure 27: Performance under dynamic scenarios.

from 12cm to 20cm. Under each inter-group distance, we change the inter-group d_{Inner} distance from 4cm to 12cm. The results obtained under different combinations of d_{Inter} and d_{Inner} are shown in Fig. 21. A lighter color means a higher grouping accuracy.

As can be seen, TaGroup achieves a higher than 95% accuracy as long as $d_{Inter} > d_{Inner}$, and achieves a 100% accuracy as long as $d_{Inter} - d_{Inner} > 2cm$. Besides, although in the case where $d_{Inter} = d_{Inner}$, TaGroup can still achieve a higher than 90% accuracy. This is because that TaGroup can group each tag based on its proximity relations with multiple tags. So, although a tag shows falsely high proximity to an incorrect set initially, it will finally bias to the correct set by considering its proximity relations with more tags, as we have mentioned in Sec. 5.3.

7.6.3 Accuracy v.s. antenna-to-tag distance. In this experiment, we observe how antenna-to-tag distance affects the grouping accuracy. We group 30 and 60 tags to 3 groups, under each number of tags, we change the antenna-to-tag distance from 1m to 2.5m. The results are shown in Fig. 22. As can be seen, TaGroup can always achieve a 100% grouping accuracy when the distance is lower than 2 m. In the case with 60 tags, the accuracy decreases to 90% when the distance increases to 2.5m . Note that a 2m inventory distance is easy to hold in most inventory applications. For example, in an self-checkout system, the distance between the shopping basket and the scanner is usually lower than 1m. In the inventory tracking system used in warehouses and logistics, the readers are usually deployed on both the right and left part of the scanning gate, where the inventory distance is usually lower than 1.5m.

7.6.4 Impact of the container material. We further observe how the container's material affects the grouping accuracy. We in this experiment use three types of containers: the plastic baskets, the cardboard boxes, and the cloth shopping bags. We put 30 and 60 tags into three containers, and attach each container with two reference tags. The performance in using different containers are shown in Fig. 23. We can see that the performance decreases slightly when we use shopping bags as containers. This is because the tags suffers a more serious orientation randomness in a shopping bag than in the other two types of containers.

7.6.5 Impact of tag arrangement. In this experiment, we evaluate the impact of tag arrangement. We consider three different scenarios: i) horizontal, where the tags are parallel to the ground; ii) vertical, where the tags are placed side-by-side, and iii) random orientated. In each scenario, we test TaGroup's performance in grouping 30 and 60 tags into three groups. Fig. 24 shows the result. As can be seen, tag arrangement does not have an apparent impact on the grouping accuracy. TaGroup can still achieve a higher than 94% accuracy when the tags are randomly placed in the container. This performance is achieved due to TaGroup's ability to group each tag based on its proximity relation to multiple tags, which mitigates the impact of tag orientation.

7.6.6 Impact of obstacles. We further evaluate TaGroup's performance under occlusion scenarios. In the experiment,

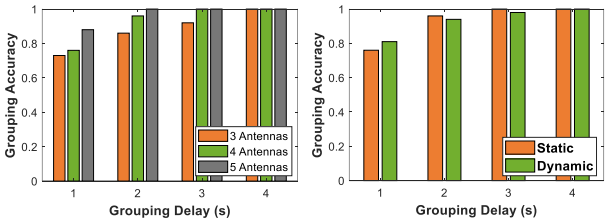

(a) Static Scenario (b) Static v.s. Dynamic scenarios

Figure 28: Accuracy v.s. grouping delay.

we block the tag-to-reader channel with three different obstacles: i) a 40×50×0.5cm^3 PMMA plate (C1), ii) a 50×50×2cm^3 foam board (C2), and iii) a 21×28×1.2cm^3 book (C3). Fig. 25 shows the results, which tell that: i) the presence of an obstacle does not obviously decrease the grouping accuracy of TaGroup; ii) the grouping accuracy changes with the material of the obstacle. In general, the grouping accuracy keeps higher than 94% in the occlusion scenarios.

7.6.7 Impact of uneven distribution of the tags. In the previous experiments, we always equally distribute the tags into different containers. Consider that in a practical RFID inventory application, tags may be unevenly distributed in different containers, we in this experiment observe how the uneven distribution of the tags affect TaGroup's performance. We put 60 tags into two containers with three different distributions: 10+50; 20+40; and 30+30. Fig. 26 shows the results obtained under different tag distributions. The results show that the uneven distribution of tags do not have apparent impact on TaGroup's performance.

7.7 Performance in dynamic scenarios

In this section, we evaluate TaGroup with 3 volunteers each carrying a bag of 15 items that are randomly placed in the bags. We let the volunteers move simultaneously in front of the querying antennas with a moving speed of 0.5m/s, during which the reader queries the tags in their bags and TaGroup groups the tags based on the query results. Fig. 27 shows the results obtained with different numbers of antennas. As can be seen, the accuracy reaches 100% when we use 2 antennas.

TaGroup achieves high accuracy even in dynamic scenarios because that, in the moving case, no matter how the tags move during the inventorying process, the tags in the same container can always stay in close proximity to each other over time. This relationship can be captured by our spatio-temporal graph model PRG.

7.8 Grouping speed

We in this section evaluate TaGroup's grouping speed. Specifically, we put 120 tags into 4 boxes, each contains 30 tags. We group these tags with 3 ∼ 5 antennas. For each number of antennas, we let the reader query the tags for 1 ∼ 4 seconds. Fig. 28 (a) shows the accuracy obtained based on the proximity relation information collected across different time scales and with different numbers of antennas.

In the figure, we can observe an obvious tradeoff between time overhead and deployment cost. When we use only 3 antenna, TaGroup has to rely on the information collected over 4s to achieve a perfect 100% grouping accuracy. While in the case with 5 antennas, the grouping latency can be reduced to 2s. So, in the applications which care more about the grouping delay (e.g., inventory tracking in logistic, where hundreds of tags should be grouped within seconds), we can improve the grouping rate by adding more antennas. While in the cases like self-checkout in small grocery, where consumers usually checkout with only several items, we can use only one antenna to save the cost.

We further perform an experiment to evaluate TaGroup's grouping speed under dynamic scenarios. In the experiment, we put 120 tags into 4 boxes and move the tags in front of the antenna with a speed of 0.5m/s. We group these tags with 4 antennas. Fig. 28 (b) compares the accuracy obtained under different grouping delay. In the result, we do not observe apparent impact of tags' mobility. In some cases (e.g., when we use the signal collected within 1s), tags' mobility can even bring a higher grouping accuracy. This is because that the movement of the tags provides an opportunity to collect tags' signals from different spatial locations and combine those signals to achieve higher accuracy.

8 CONCLUSIONS

We in this paper presents TaGroup, a fast, fine-grained, and robust grouping technique for RFIDs. The core of TaGroup is a novel technique which can accurately and simultaneously estimate the proximity relation between multiple pairs of tags, based on which TaGroup can build a spatio-temporal graph model that captures a full picture of proximity relation among all the tags. This graph enables TaGroup to perform a robust grouping of the tags. We believe that the application of such an proximity detection method extends beyond RFID grouping. It paves the way for exciting new avenues for exploration in RFID sensing.

9 ACKNOWLEDGMENT

We thank our shepherd and the anonymous reviewers for their constructive feedback. This work was supported by the National Key Research and Development Program of China under Grant 2020YFB1708700. National Natural Science Fund of China (62272293,42050105).

REFERENCES

[1] C. Jiang and Y. He, X. Zheng, and Y. Liu. 2021. OmniTrack: Orientation-aware RFID Tracking with Centimeter-level Accuracy. *IEEE Transactions on Mobile Computing* 20, 2 (2021).

[2] C. Bocanegra, M. Amir, M. Y. Arslan, E. Chai, S. Rangarajan, and K. R. Chowdhury. 2020. RFGo: A Seamless Self-checkout System for Apparel Stores Using RFID. In *MobiCom*.

[3] T. Boroushaki, I. Perper, M. Nachin, A. Rodriguez, and F. Adib. 2021. RFusion: Robotic Grasping via RF-Visual Sensing and Learning. In *SenSys*.

[4] C. Duan, J. Liu, X. Ding, Z. Li, and Y. Liu. 2021. Full-Dimension Relative Positioning for RFID-Enabled Self-Checkout Services. In *UbiComp*.

[5] G. M. Gaukler. 2011. Item-Level RFID in a Retail Supply Chain with Stock-Outbased Substitution. *IEEE Transactions on Industrial Informatics* (2011).

[6] J. Han, C. Qian, X. Wang, D. Ma, J. Zhao, W. Xi, Z. Jiang, and Z. Wang. 2015. Twins: Device-free Object Tracking using Passive Tags. *IEEE Transactions on Networking* 24, 3 (2015).

[7] Y. He, Y. Zheng and M. Jin and S. Yang, X. Zheng, and Y. Liu. 2021. RED: RFID-based Eccentricity Detection for High-speed Rotating Machinery. *IEEE Transactions on Mobile Computing* 20, 4 (2021).

[8] P. Hu, P. Zhang, and D. Ganesan. 2015. Laissez-Faire: Fully Asymmetric Backscatter Communication. In *SIGCOMM*.

[9] H. Jiang, J. Zhang, X. Guo, and Y. He. 2021. Sense Me on the Ride: Accurate Mobile Sensing over a LoRa Backscatter Channel. In *ACM SenSys*.

[10] M. Jin, Y. He, C. Jiang, and Y. Liu. 2020. Fireworks: Channel Estimation of Parallel Backscattered Signals. In *IPSN*.

[11] M. Jin, Y. He, X. Meng, Y. Zheng, D. Fang, and X. Chen. 2017. FlipTracer: Practical Parallel Decoding for Backscatter Communication. In *MobiCom*.

[12] M. Jin, S. Yao, K. Li, X. Tian, X. Wang, C. Zhou, and X. Cao. 2022. A Passive Eye-in-Hand "Camera" for Miniature Robots. In *ACM SenSys*.

[13] N. Kargas, F. Mavromatis, and A. Bletsas. 2015. Fully-coherent Reader with Commodity SDR for GEN2 FM0 and Computational RFID. *IEEE Wireless Communications Letters* (2015).

[14] Z. Luo, Q. Zhang, Y. Ma, M. Singh, and F. Adib. 2019. 3D Backscatter Localization for Fine-Grained Robotics. In *NSDI*.

[15] D. Ma, C. Qian, W. Li, J. Han, and J. Zhao. 2013. GenePrint: Generic and Accurate Physical-Layer Identification for UHF RFID Tags. In *ICNP*.

[16] Y. Ma, N. Selby, and F. Adib. 2017. Minding the Billions: Ultra-wideband Localization for Deployed RFID Tags. In *MobiCom*.

[17] L. Ni, Y. Liu, Y. Lau, and A. Patil. 2004. Landmarc: Indoor Location Sensing Using Active RFID. *Wireless networks* 10, 6 (2004).

[18] J. Ou, M. Li, and Y. Zheng. 2015. Come and Be Served: Parallel Decoding for COTS RFID Tags. In *MobiCom*.

[19] L. Shangguan, Z. Zhou and X. Zheng, L. Yang, Y. Liu, and J. Han. 2015. ShopMiner: Mining customer shopping behavior in physical clothing stores with COTS RFID devices. In *ACM SenSys*.

[20] L. Shangguan and K. Jamieson. 2016. The Design and Implementation of a Mobile RFID Tag Sorting Robot. In *MobiSys*.

[21] L. Shangguan, Z. Yang, A. Liu, Z. Zhou, and Y. Liu. 2015. Relative Localization of RFID Tags using Spatial-temporal Phase Profiling. In *NSDI*.

[22] C. Wang, L. Xie, W. Wang, T. Xue, and S. Lu. 2016. Moving Tag Detection via Physical Layer Analysis for Large-Scale RFID Systems. In *INFOCOM*.

[23] G. Wang, H. Cai, C. Qian, J. Han, X. Li, and H. Ding. 2018. Towards Replay-resilient RFID Authentication. In *MobiCom*.

[24] J. Wang, O. Abari, and S. Keshav. 2018. RFID Hacking for Fun and Profit. In *MobiCom*.

[25] J. Wang, F. Adib, R. Knepper, D. Katabi, and D. Rus. 2013. RF-Compass: Robot Object Manipulation Using RFIDs. In *MobiCom*.

[26] J. Wang, H. Hassanieh, D. Katabi, and P. Indyk. 2012. Efficient and Reliable Low-Power Backscatter Networks. In *SIGCOMM*.

[27] J. Wang and D. Katabi. 2013. Dude, Where's My Card? RFID Positioning That Works with Multipath and Non-Line of Sight. In *SIGCOMM*.

[28] J. Wang, J. Xiong, H. Jiang, X. Chen, and D. Fang. 2018. D-Watch: Embracing "bad" Multipaths for Device-Free Localization with COTS RFID Devices. In *CoNext*.

[29] T. Wei and X. Zhang. 2016. Gyro in the Air: Tracking 3D Orientation of Batteryless Internet-of-Things. In *MobiCom*.

[30] B. Xie, J. Xiong, X. Chen, E. Chai, L. Li, Z. Tang, and D. Fang. 2019. Tagtag: Material Sensing with Commodity RFID.. In *ACM SenSys*.

[31] B. Xie, J. Xiong, X. Chen, and D. Fang. 2020. Exploring Commodity RFID for Contactless Sub-millimeter Vibration Sensing. In *SenSys*.

[32] J. Xu, W. Sun, A. Bakshi, and K. Srinivasan. 2020. Embracing collisions: Enabling Parallel Channel Estimation with COTS Passive Backscatter Tags. In *LIOT*.

[33] L. Yang, Y. Chen, X. Li, C. Xiao, M. Li, and Y. Liu. 2014. Tagoram: real-time tracking of mobile rfid tags to high precision using cots devices. In *MobiCom*.

[34] D. Zanetti, B. Danev, and S. Capkun. 2010. Physical-layer Identification of UHF RFID Tags. In *MobiCom*.

[35] Z. Zhou, L. Shangguan and X. Zheng, L. Yang, and Y. Liu. 2017. Design and Implementation of an RFID-based Customer Shopping Behavior Mining System. *IEEE/ACM Transactions on Networking* 25, 4 (2017).